Mechanical Systems and Signal Processing 215 (2024) 111416

Contents lists available at ScienceDirect

Mechanical Systems and Signal Processing

journal homepage: www.elsevier.com/locate/ymssp

Inverse surrogate model for deterministic structural model updating based on random forest regression

S. Kamali [a,b], S. Mariani [a], M.A. Hadianfard [b], A. Marzani [a,*]

[a] Department of Civil, Chemical, Environmental and Materials Engineering, University of Bologna, Bologna, Italy
[b] Department of Civil and Environmental Engineering, Shiraz University of Technology, Shiraz, Iran

ARTICLE INFO

Communicated by J.E. Mottershead

Keywords:
Model updating
Surrogate models
Random forests
Structural health monitoring

ABSTRACT

This article presents a novel method for deterministic finite element model updating that is based on an "inverse surrogate model". The latter is a regression model that uses structural responses as independent variables and structural properties as dependent ones. Such regressor is trained on structural responses using a finite element model having in input the structural properties to be updated. The training set is obtained by executing multiple finite element model instances where each instance is formed by assigning random, though realistic, values to the structural properties. Experimentally measured structural responses can then be given as input to the trained "inverse surrogate model", and the structural properties, which are used to update the finite element model, are obtained as output. Random forest algorithm is identified as a good candidate to perform this type of regression, and the performance offered by this method is compared to that of the "standard" finite element model updating based on the particle swarm optimization algorithm on both a numerical and an experimental case study where the structural responses are represented by a set of modal parameters. The results show that the proposed approach offers higher accuracy on the estimation of the structural properties, at the cost of a slightly inferior matching of the modal parameters. This indicates that the "inverse surrogate model" is less susceptible to the ill-conditioning issue that plagues optimization-based finite element model updating, where similar structural responses can arise from various combinations of structural properties. The results also show a good repeatability and that the computational costs are similar or better than those of the particle swarm optimization algorithm.

1. Introduction

The aging of civil structures and infrastructures has recently prompted significant interest in the design and operation of structural health monitoring (SHM) systems [1–3]. This often involves the development of a finite element model (FEM) of the monitored structure that can be used to predict its response under damaged conditions. Building a numerical model that faithfully mimics the actual structural behavior is a challenging task due to a number of factors such as uncertainties related to material properties and boundary conditions, deviations from original design drawings, or the actions of external agents such as fatigue, humidity, and corrosion. For this reason, iterative procedures are typically employed to calibrate some of the parameters of the model in order to minimize the differences between measured structural responses and the model's outputs. This process is generally termed finite element model updating (FEMU) [4]. Natural frequencies and mode shapes are among the structural responses generally used for

* Corresponding author.
E-mail address: alessandro.marzani@unibo.it (A. Marzani).

https://doi.org/10.1016/j.ymssp.2024.111416
Received 16 January 2024; Received in revised form 29 March 2024; Accepted 9 April 2024
Available online 16 April 2024

List of acronyms and symbols

BA	Bees Algorithm
FEM	Finite Element Model
FEMU	FEM updating
FRF	Frequency Response Function
GA	Genetic Algorithm
$\mathbf{l}_y$	Lower bound vector of the structural parameters
M	Number of target variables
MAC	Modal Assurance Criterion
ML	Machine Learning
N	Number of features
NM	Nelder–Mead Simplex
OMA	Operational Modal Analysis
OOB	Out of Bag data
P	Number of features for sub-sampling phase
PSO	Particle Swarm Optimization
RF	Random Forest
SHM	Structural Health Monitoring
SOMI	Spectral Optimization-based Modal Identification
SQP	Sequential Quadratic Programming
S	Sample space size
$\mathbf{B}$	The bootstrap sample
$\mathbf{x}$	A sample of features
$\mathbf{y}$	A sample of target variables
$\hat{\mathbf{x}}$	An experimental sample of features
$\hat{\mathbf{y}}$	A sample of predicted target variables
$\mathbf{X}$	The matrix of sample features
$\mathbf{Y}$	The matrix of sample target variables
$\mathbf{u}_y$	Upper bound vector of the structural parameters
g	The actual model
$\hat{g}$	The regression model
n_l	Minimum number of samples in leaf
n_t	Number of decision trees

FEMU procedures. These are obtained via eigenvalue analysis on the FEM, and can be estimated on the actual structure by collecting vibration data and by then performing operational modal analysis (OMA) [5].

A vast number of different FEMU strategies are found in literature, virtually all of which can be classified either as deterministic or stochastic approaches [6]. The former are setup as optimization problems in which the unknown parameters are treated as unknown-but-fixed constants, and an objective function is defined in terms of residuals between numerical and experimental datasets. Stochastic methods, instead, consider the unknown parameters as random variables and aim to quantify their uncertain distribution [7]. These methods can be based either on frequentist or on Bayesian approaches. The former make use of optimization techniques framed in a stochastic scenario, where the minimizing object is a set of frequentist properties such as mean and covariance of the data [8]. In the Bayesian framework, instead, the prior distributions of the parameters to be calibrated are first hypothesized, then a likelihood function is derived from the observed experimental data, and this information is used to update the posterior probability [9]. While stochastic approaches can yield superior results, they require a vast amount of experimental data and are typically computationally very intensive [6]. Therefore, deterministic methods are still widely used in practical applications. Also, several probabilistic model updating approaches incorporate deterministic methods into their algorithms. For these reasons, this article focuses on deterministic approaches.

Some of the most significant works published in the field of FEMU via deterministic approaches in the last decade are summarized in the following. In 2010, Moradi et al. [10] estimated the modal parameters of a piping system by performing a hammer test and by extracting the frequency response function (FRF) of an accelerometer. They then developed a FEM of the structure and setup a FEMU procedure where the objective function was the weighted sum of the squared error between FEM and experimental modal parameters. Finally, they compared the performance of different optimization algorithms, namely bees algorithm (BA) [11], genetic algorithm (GA) [12], particle swarm optimization (PSO) [13] and the inverse eigensensitivity method [14]. Their analysis showed that BA and PSO yield very similar results and outperform the other methods. In the same year, Marwala [15] compared GA and

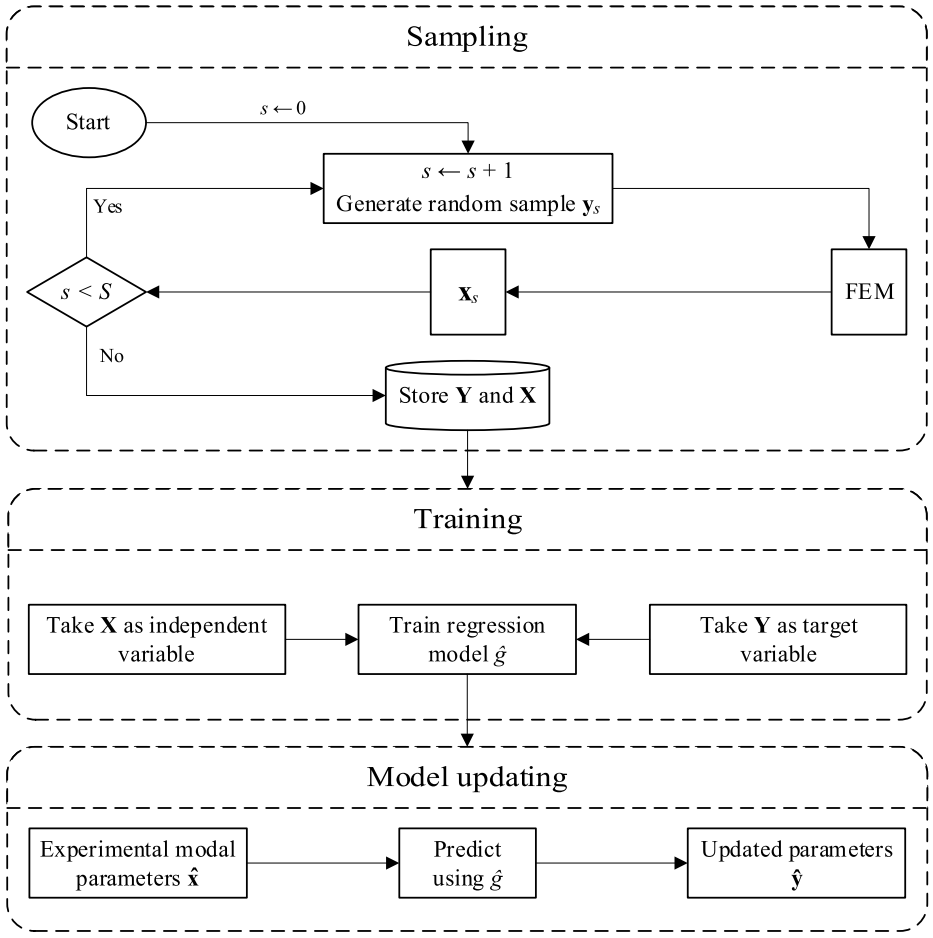

Fig. 1. Flowchart of the proposed FEMU procedure.

PSO for fault identification and model updating of simply supported beams, also concluding that PSO outperforms GA. They further showed that a combination of Nelder–Mead Simplex (NM) method [16] and PSO is highly effective for fault detection, if PSO and NM are used for global and local optimization, respectively. In 2016, Zhang et al. proposed a FEMU method for damage identification based on a combination of multivariable wavelet FEM and PSO [17]. Additional examples of recent research on deterministic FEMU involving a variety of optimization algorithms are given in [18–25].

One of the limitations of FEMU is that performing FEM dynamic analysis is a time-consuming process [26]. To address this challenge, some researchers have proposed to replace FEMs with surrogate models in order to expedite the model updating process. Surrogate models are mathematical functions used to express the relationships between the FEM response and the updating parameters. These functions can take various forms, such as neural network regression models [27], Kriging models [26,28,29], radial basis function [30], or adaptive Gaussian surrogate models [31]. Another limitation of FEMU approaches is that the problem they are trying to solve is often ill-conditioned, i.e. there exist multiple combinations of the FEM updating parameters that yield a similarly low value for the objective function. This has been investigated by Simoen et al. [32] on a reinforced concrete beam. In their study, six different stiffness patterns along the beam yielded almost identical modal properties. They also showed that minor alterations in measurements or model predictions could result in widely different model updating outcomes. Regularization techniques [33] are often used to limit the ill-conditioning issue. The purpose of regularization in inverse analysis is to emphasize particular regions within the parameter space where the solutions of the model are expected to be found [34]. However, regularization techniques often require manual hyper-parameters tuning, such as the regularization term, through methods like cross-validation, which can be time-consuming, especially in complex problems. Furthermore, an improper choice of the regularization strength can introduce bias, potentially leading to underfitting or overfitting issues, hence impacting the predictive and generalization performance [35].

This work postulates that the ill-conditioning issue can be mitigated if the mutual relationships between the different natural frequencies and mode shapes are also taken into account. This would restrict the space in which solutions to the optimization problem are sought. In order to achieve this, a novel FEMU procedure based on the random forest (RF) algorithm [36] is proposed.

As a first step, lower and upper bounds for the various geometric and mechanical parameters to be updated are defined. Then, the FEM is solved several times by assigning values to the parameters that are picked at random within the respective boundaries. At each run, modal frequencies and mode shapes are computed and stored in a database. Finally, RF is employed to generate a regression model between the modal responses, considered as the independent variables, and the FEM updating parameters, considered as the dependant variables. Once such regressive surrogate model is trained, when a new set of experimental modal responses is obtained, that is given to the regression model as input in order to predict the FEM updated parameters that are expected to produce such modal output. Such regression model is referred to as "inverse surrogate model" since it reverses the roles of inputs and outputs when compared to the FEM, for which mechanical and geometrical parameters are the inputs and modal responses are the outputs.

The performance of the proposed procedure is compared to that offered by the "classic" deterministic FEMU based on PSO, which is arguably the most commonly used optimization algorithm for FEMU [6], on a numerical and an experimental case studies. The former is a two-dimensional (2D) FEM of a truss that was presented in [37], while the latter is the experimental structure discussed in [38].

The remainder of the article is structured as follows. Section 2 presents the proposed inverse surrogate model based on RF for FEMU. Section 3 discusses the two case studies and compares the performance obtained via the proposed method to that of PSO, both in terms of accuracy and repeatability of the results. Finally, Section 4 concludes the article by summarizing the key findings.

2. Methodology

2.1. Proposed procedure for FEMU

The proposed FEMU procedure is summarized in Fig. 1, and it is described in the following:

1. A number M of FEM "target" structural parameters to be updated are defined. These are typically some geometric and/or mechanical properties of the elements composing the model.
2. For each target parameter, admissible lower and upper bounds are defined:
$$\begin{aligned} \mathbf{l}_y &= [l_1, l_2, \dots, l_M] \\ \mathbf{u}_y &= [u_1, u_2, \dots, u_M] \end{aligned} \tag{1}$$
where $\mathbf{l}_y \in \mathbb{R}^M$ and $\mathbf{u}_y \in \mathbb{R}^M$ are vectors collecting all the lower and upper bounds, respectively.
3. The "sampling" phase of Fig. 1 is initiated. A number S of $\mathbf{y}_s \in \mathbb{R}^M$ vectors, each containing a set of values picked at random within their respective boundaries and assigned to the target parameters, are generated as:
$$\mathbf{y}_s = \mathbf{l}_y + (\mathbf{u}_y - \mathbf{l}_y) \cdot \mathbf{r} \tag{2}$$
where $s = [1 \text{ to } S]$, and $\mathbf{r} \sim \mathcal{U}_M(\mathbf{0}, \mathbf{1})$ is a vector of M random numbers with standard uniform distribution that is re-drawn at each sample s.
4. For each sample s, the $\mathbf{y}_s$ parameters are assigned to the FEM, and a number N of structural responses are computed and collected as:
$$\mathbf{x}_s = [x_{s1}, x_{s2}, \dots, x_{sN}] \tag{3}$$
Note that in this article only modal data, i.e. solely natural frequencies or natural frequencies and mode shapes, were considered as structural responses.
5. All vectors $\mathbf{x}_s$ and $\mathbf{y}_s$ are collected to form a "feature" matrix $\mathbf{X} = \{\mathbf{x}_s\}_{s=1}^{S}$ ($\mathbf{X} \in \mathbb{R}^{S \times N}$) and a "target" matrix $\mathbf{Y} = \{\mathbf{y}_s\}_{s=1}^{S}$ ($\mathbf{Y} \in \mathbb{R}^{S \times M}$). Then, in the "training" phase of Fig. 1 a regression model ($\hat{g}$) is trained so that:
$$\mathbf{Y} \simeq \hat{g}(\mathbf{X}) \tag{4}$$
6. Once the regression model is trained, the "model updating" phase of Fig. 1 can initiate. At this stage, when a new set of experimental structural responses (OMA modal data in this work) $\hat{\mathbf{x}} \in \mathbb{R}^N$ is obtained, the FEM is updated by assigning to it the set of updated target parameters $\hat{\mathbf{y}}$ obtained as:
$$\hat{\mathbf{y}} = \hat{g}(\hat{\mathbf{x}}) \tag{5}$$

2.2. Regression via random forest algorithm

The term "regression" refers to statistical techniques used to model the relation between some target variables and some other input features. In this work, the regression task is performed with the RF algorithm [36,39]. This is an ensemble machine learning (ML) method [40] that constructs a multitude of decision trees [41] during its training phase and that averages their predictions at testing time. In particular, given the full set of training data that includes S samples for both input ($\mathbf{X} \in \mathbb{R}^{S \times N}$) and output ($\mathbf{Y} \in \mathbb{R}^{S \times M}$) variables, a procedure called "bootstrap aggregation" [42] is used to build each decision tree, for which only a subset $L \leq S$ of the available input samples are randomly selected and used. Note that in this procedure any given sample can be re-used in multiple decision trees.

Each tree is constructed starting with a "root node" that holds the corresponding bootstrap input sample $\mathbf{B} \in \mathbb{R}^{L \times N}$. The next step is to split the root node in two child nodes and to define a "splitting criterion" used to assign all samples to either of them in such a way that the total "entropy" of the two nodes, as measured by the "Gini Index" [42], is minimized. Practically, the splitting criterion is represented by a specific threshold set on a single feature chosen among a randomly selected subset P of the N total features, based on a technique called "feature sub-sampling" [43]. In this work, P is set to $N/3$ as suggested in literature for regression tasks [40]. This procedure continues in recursive manner from each child node until a predefined "stopping criterion" is met [42], at which point "leaf nodes" are formed, which represent the final predictions of the decision tree. A widely used stopping criterion is to form a leaf node when its total number of samples are below a set value n_l. A recommended value for n_l in regression tasks is five [40], hence this is adopted in this work.

The entire procedure is iteratively repeated until a set number n_t of decision trees are constructed, at which point the random forest training is complete. Then, at testing time, the new input sample is processed through all the decision trees in the random forest, resulting in n_t individual outputs. The final prediction is obtained by averaging all these individual tree predictions. To summarize the employed random forest regression described above, its pseudo-code implementation is presented in Algorithm 1.

Algorithm 1 Random forests for regression

Input: Dataset of size S, number of trees n_t, number of features N, minimum samples in leaf n_l.

procedure RandomForests(S, n_t, N, n_l)
  for $i = 1$ to n_t **do**
    Extract a bootstrap sample with size $L \leq S$.
    Build decision tree T_i using the bootstrap sample as follows:
      $T_i \leftarrow$ **BuildTree**(node = 1, samples = bootstrap, N)
  end for
  return ensemble of trees $\{T_i\}_{i=1}^{n_t}$.
end procedure

procedure BuildTree(node, samples, N)
  if length(samples) $< n_l$ **then**
    Make the node a leaf.
  else
    Select $P = N/3$ features at random from the N features.
    Select the best variable and its splitting threshold.
    Split node into two child nodes (left and right).
    left_child_samples ← samples satisfying splitting criterion.
    right_child_samples ← samples not satisfying splitting criterion.
    BuildTree(left_child_node, left_child_samples, N)
    BuildTree(right_child_node, right_child_samples, N)
  end if
end procedure

To make a prediction at a new point $\hat{\mathbf{x}}$:
  $\{T_i\}_{i=1}^{n_t} \leftarrow$ **RandomForests**(S, n_t, N, n_l)
  $\hat{\mathbf{y}}(\hat{\mathbf{x}}) \leftarrow \frac{1}{n_t} \sum_{i=1}^{n_t} T_i(\hat{\mathbf{x}})$

Notably, random forests do not require the explicit formation of a testing set to be used for an unbiased estimation of the performance on unseen data. In fact, this can be done on the so-called out-of-bag (OOB) data, i.e. the samples that were not utilized in the construction of a particular decision tree as a result of bootstrapping. Therefore, for each decision tree the accuracy of regression on the respective OOB samples is evaluated, and ultimately the mean squared error of the accuracies yield by all decision trees are averaged to give an indication of the overall performance of the RF model. Furthermore, by plotting the OOB performance against the number of trees one can define an "optimal" n_t value by identifying a point at which further increasing the number of trees does not lead to significant improvements [44].

Other advantages of RF over competitor ML regression algorithms are (1) its ability to automatically handle missing variables in the input samples, (2) the fact that it does not require manual feature normalization, since all features are independently considered for splitting decisions, and (3) its robustness to outliers, since the combination of multiple decision trees averages out their impact [40,42,43].

3. Case studies

3.1. Case study I: 2D FEM of a statically determinate truss

The 2D FEM of the statically determinate truss depicted in Fig. 2 and presented in Section 3.1 of a previous work by two of the authors [37] is used as a first numerical case study in this work. The parameters of all truss elements are: Young's modulus

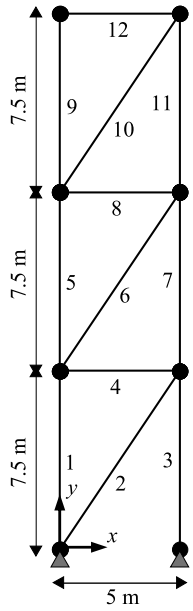

Fig. 2. 2D FEM truss presented in Section 3.1 of [37]. The truss is restrained at the base nodes with hinged supports.

Table 1
Lower bounds, upper bounds, and true values of the design variables for all elements.

Parameter	Lower bound	True value	Upper bound
E (GPa)	50.19	71.7	93.21
ρ (kg/m^3)	1937.6	2768	3598.4
A (m^2)	0.000007	0.00001	0.000013

E = 71.7 GPa, mass density ρ = 2768 kg/m^3, and cross-sectional area $A = 10^{-5}$ m^2. The modal parameters, namely frequencies and mode shapes, obtained in [37] using the spectral optimization-based modal identification (SOMI) method are considered as the experimental modal data. The twelve natural frequencies are $\mathbf{f}$ = [7.31, 24.24, 41.95, 42.61, 81.6, 117.61, 120.01, 138.92, 146.49, 154.05, 167.97, 186.49] rad/s.

In this study, it is assumed that the values of E, ρ, and A of all elements are unknown, and the goal is to perform a FEMU procedure where they are adjusted in order to minimize the differences between the experimental modal parameters (i.e. those estimated by SOMI on the original model) and those computed by the updating model. It is also assumed that the possible values for the 36 target parameters denoted as E_1, E_2, …, E_{12}, ρ_1, ρ_2, …, ρ_{12}, and A_1, A_2, …, A_{12}, where the indices correspond to element numbers, are to be sought within a +/- 30% variation from their true values, as suggested in [5], and these ranges are listed in Table 1. This task is performed both via a "classic" optimization-based FEMU using PSO, and with the proposed inverse surrogate model based on RF, so that the results of the two methods can be compared. Furthermore, for both approaches two scenarios are considered, one where only the modal frequencies are assumed available, and the other one where both modal frequencies and mode shapes are taken into account.

Prior to model updating, sensitivity analyses are generally performed to find those structural parameters that have the highest influences in the updating process [24]. In the present case, a sensitivity analysis regarding variations in E, ρ, and A for all elements is performed in order to understand whether all 36 target parameters can have a significant influence on the modal responses. The normalized sensitivity (κ) of any modal frequency ω to a specific parameter p is defined as:

$$\kappa = \frac{\partial \omega}{\partial p} \cdot \frac{p}{\omega} \tag{6}$$

where $\frac{\partial \omega}{\partial p}$ represents the partial derivative of ω with respect to p. For example, the sensitivity of the ith modal frequency component to variations in the Young's modulus of the jth element (E_j) from its true value of E = 71.7 GPa is obtained as:

$$\kappa(\omega_i, E_j) = \frac{\partial \omega_i}{\partial E_j} \cdot \frac{E_j}{\omega_i} \tag{7}$$

where the partial derivative is computed via the following finite difference approximation:

$$\frac{\partial \omega_i}{\partial E_j} \simeq \frac{\omega_i(E_j + \Delta E_j) - \omega_i(E_j)}{\Delta E_j} \tag{8}$$

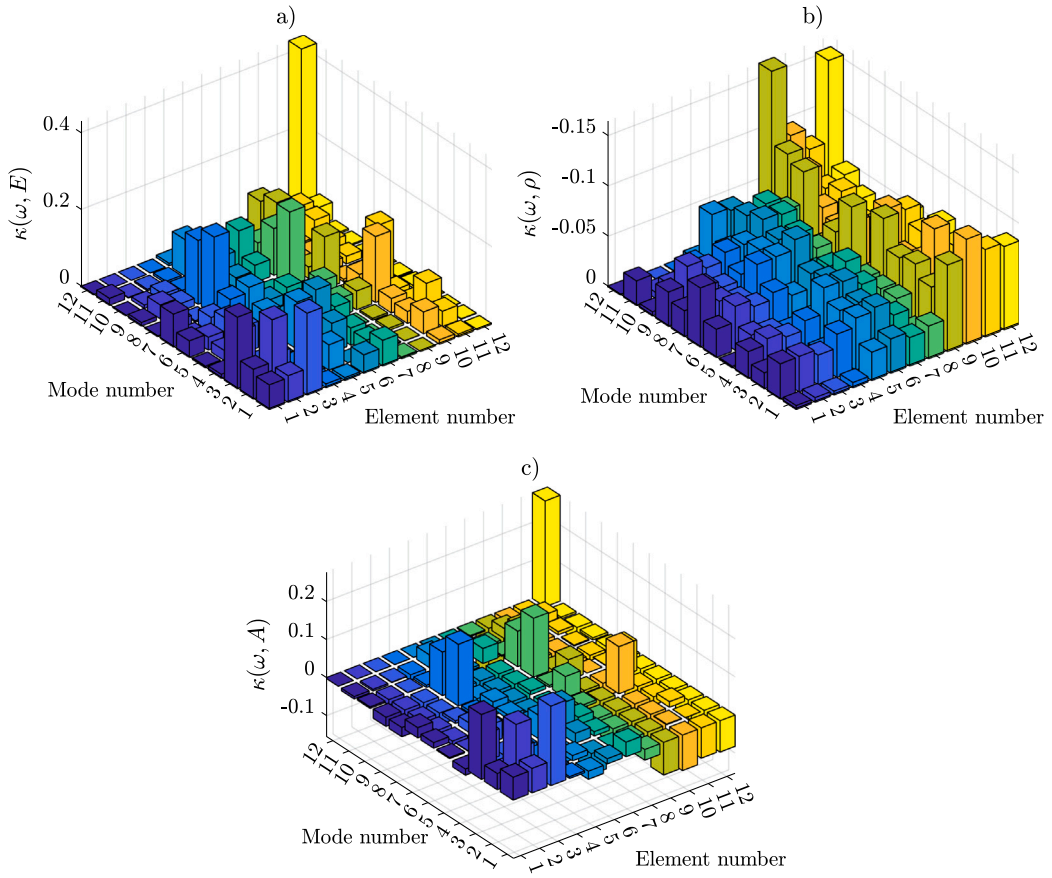

Fig. 3. Normalized sensitivity of modal frequencies to variations in E (a), ρ (b) and A (c) of the truss elements.

with ΔE_j being a small positive change. All results are plotted in Fig. 3. The plots show that all parameters have a significant influence on at least a single modal frequency, and, therefore, they are all considered for the FEMU procedures described in the following.

3.1.1. Case study I: model updating using PSO

FEMU using PSO [13] is performed twice using the following two objective functions [45]:

$$O_1 = \sum_{i=1}^{N} \left(\frac{\omega_i - \hat{\omega}_i}{\hat{\omega}_i} \right)^2 \tag{9}$$

$$O_2 = \sum_{i=1}^{N} \left(\frac{\omega_i - \hat{\omega}_i}{\hat{\omega}_i} \right)^2 + \sum_{i=1}^{N} \left(1 - \mathrm{MAC}_i\right) \tag{10}$$

where ω_i and $\hat{\omega}_i$ are the ith updating model and experimental frequencies, respectively, and MAC_i is the modal assurance criterion for the ith mode, often used to indicate similarity of two mode shapes, defined as:

$$\mathrm{MAC}_i = \frac{|\boldsymbol{\phi}_i^T \hat{\boldsymbol{\phi}}_i|^2}{(\boldsymbol{\phi}_i^T \boldsymbol{\phi}_i)(\hat{\boldsymbol{\phi}}_i^T \hat{\boldsymbol{\phi}}_i)} \tag{11}$$

where $\boldsymbol{\phi}_i$ and $\hat{\boldsymbol{\phi}}_i$ are the ith normalized mode shape vectors from the updating model and the experiment, respectively. As the formula implies, MAC_i is a number between 0 and 1, where the two limits correspond to the two mode shape vectors being orthogonal or identical to each other, respectively.

Table 2 summarizes the settings used to perform the PSO algorithm in *MATLAB*, while Fig. 4 plots the histories of the objective functions until both iterations are stopped since improvements higher than the "function tolerance" value were not recorded over the latest 20 iterations (as defined by the "maximum stall iterations" setting). While a more detailed analysis of the results of both iterations is discussed in the following Section 3.1.3, Fig. 5 shows that the difference between experimental and updated frequencies when objective function O_2 is used is extremely small, therefore indicating that the PSO-based FEMU procedure has been well-implemented.

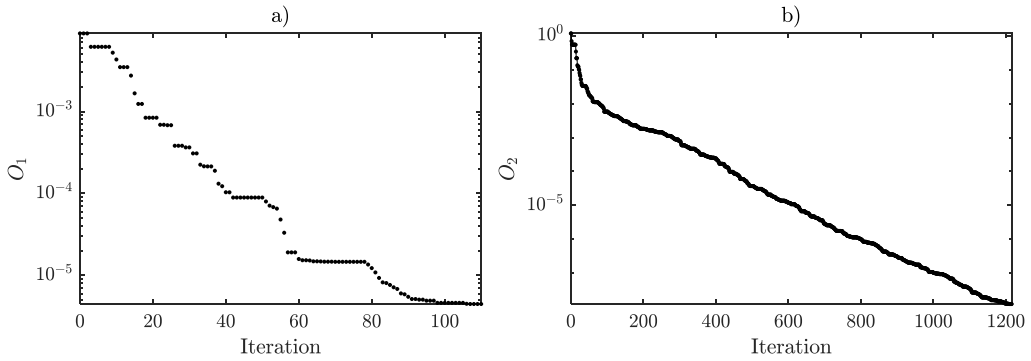

Fig. 4. Histories of the objective functions O_1 (a) and O_2 (b) during the iterations of the PSO algorithm.

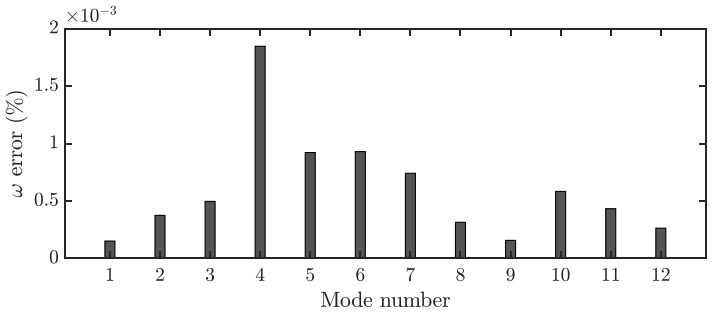

Fig. 5. Absolute difference between experimental and updated frequencies when PSO is used on the objective function O_2.

Table 2
Settings used to perform the PSO algorithm in *MATLAB*.

Parameter	Value
Initial swarm span	2000
Maximum iterations	200×36
Maximum stall iterations	20
Minimum neighbors fraction	0.25
Self-adjustment weight	1.49
Social adjustment weight	1.49
Function tolerance	1.0000e−09
Swarm size	min $(100, 10 \times 36)$
Inertia range	[0.1000, 1.1000]

3.1.2. Case study I: model updating using the proposed inverse surrogate model

Two inverse surrogate models termed $\hat{\mathbf{g}}_1$ and $\hat{\mathbf{g}}_2$ are generated using the parameters listed in Table 3. $\hat{\mathbf{g}}_1$ only uses the 12 modal frequencies, while $\hat{\mathbf{g}}_2$ considers both 12 modal frequencies and the components of the 12×12 mode shape matrix, which is formed by normalizing each mode shape vector to its first component. The OOB error analysis computed for all 36 target variables for the case of $\hat{\mathbf{g}}_2$, which is plotted in Fig. 6, shows that for all variables the error plateaus before $n_t = 100$, hence there would not be any benefit in increasing the chosen n_t value. A similar behavior is obtained for the case of $\hat{\mathbf{g}}_1$ (not shown for brevity). Once $\hat{\mathbf{g}}_1$ and $\hat{\mathbf{g}}_2$ are trained, the experimental frequencies and mode shapes are given as input to both models, and the predicted values for E, ρ, and A obtained for all elements are discussed in the next section.

3.1.3. Case study I: comparison of results

The results of the FEMU procedures performed using PSO and the inverse surrogate models based on RF are shown in Fig. 7. In particular, the first three rows of plots refer to E, ρ, and A of all elements, while the fourth row considers the modal frequencies. The left column of plots compares the predicted values to the true ones, while the right column shows the absolute errors. In all plots, blue and red colors are used for PSO when using the objective functions O_1 and O_2, respectively, yellow and purple represent inverse surrogate models $\hat{\mathbf{g}}_1$ and $\hat{\mathbf{g}}_2$, respectively, and green is used for the true values. For clarity, all quantities plotted in Fig. 7 are also listed in Tables 4 to 7.

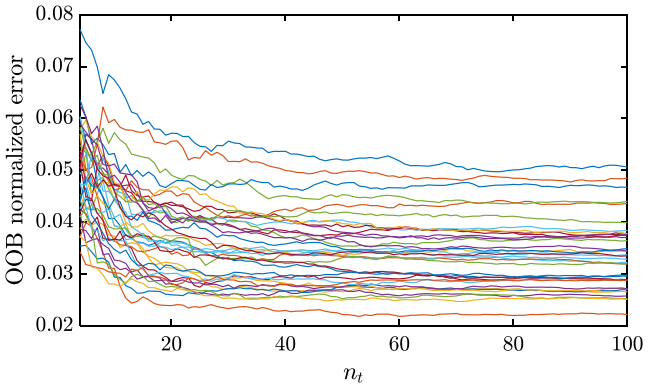

Fig. 6. OOB normalized error vs. number of trees for all 36 target parameters for $\hat{\mathbf{g}}_2$.

Table 3
Parameters used to generate the inverse surrogate models.

Parameter	Value
Number of samples (S)	100
Number of decision trees (n_t)	100
Minimum leaf size (n_l)	5

Table 4
Error (%) in the updated E of all elements.

Element	PSO (ω)	PSO (ω and ϕ)	RF (ω)	RF (ω and ϕ)
1	6.42	14.77	2.51	1.06
2	6.44	22.03	7.58	3.17
3	19.57	5.03	9.29	1.11
4	13.94	7.96	9.04	0.54
5	6.10	21.53	6.96	6.15
6	9.49	3.54	2.53	0.22
7	23.77	2.24	2.92	1.66
8	20.00	3.93	2.55	0.82
9	6.15	29.92	1.35	2.84
10	26.86	7.09	6.67	1.57
11	8.59	20.89	14.05	6.10
12	23.41	0.10	8.91	2.34
Mean	14.23	11.59	6.20	2.30

The analysis of all plots shown in Fig. 7 reveals that, on average, the predictions of the 36 target parameters E, ρ, and A made by the inverse surrogate models are more accurate than those made by the PSO algorithm, and, for both approaches, the predictions yielded when the mode shapes are also taken into account are superior to those made only considering the modal frequencies. This is well summarized in Fig. 8, where the average errors in the predictions of E, ρ, and A for all 12 elements are given (these values are also listed in the last row of Tables 4 to 6). Restricting the attention to the scenarios in which both modal frequencies and mode shapes are considered, Fig. 8 shows that there is essentially a five-fold improvement in the prediction of mechanical and geometrical properties of the elements when using the proposed method (average error between 2 and 3.5%) over the PSO algorithm (average error between 12 and 17%).

This comes at the cost of a less accurate prediction of modal frequencies, as seen in Fig. 7(h), where the errors of the PSO are barely visible at this zoom level. This is expected, since the specific goal of PSO is to minimize the differences between experimental and predicted modal responses. However, such minimization does not guarantee the accuracy of the target structural parameters, which in a few instances yielded the extreme admissible value (i.e. a 30% error), as seen in Fig. 7(b,d,f).

3.1.4. Case study I: robustness of the results and computational cost

Since the results of both FEMU procedures described in Sections 3.1.1 and 3.1.2 depend on their random initialization (the initial set of candidate solutions for PSO [13], and the set of FEM samples used for training for the inverse surrogate model), they are both repeated twenty times, and Table 8 gives mean and standard deviation of the errors on the predicted mechanical and geometrical properties of the FEM truss. The same table also reports the average time required to run a single FEMU instance on a PC mounting an Intel® Core™ i7-8565U CPU at 1.8 GHz.

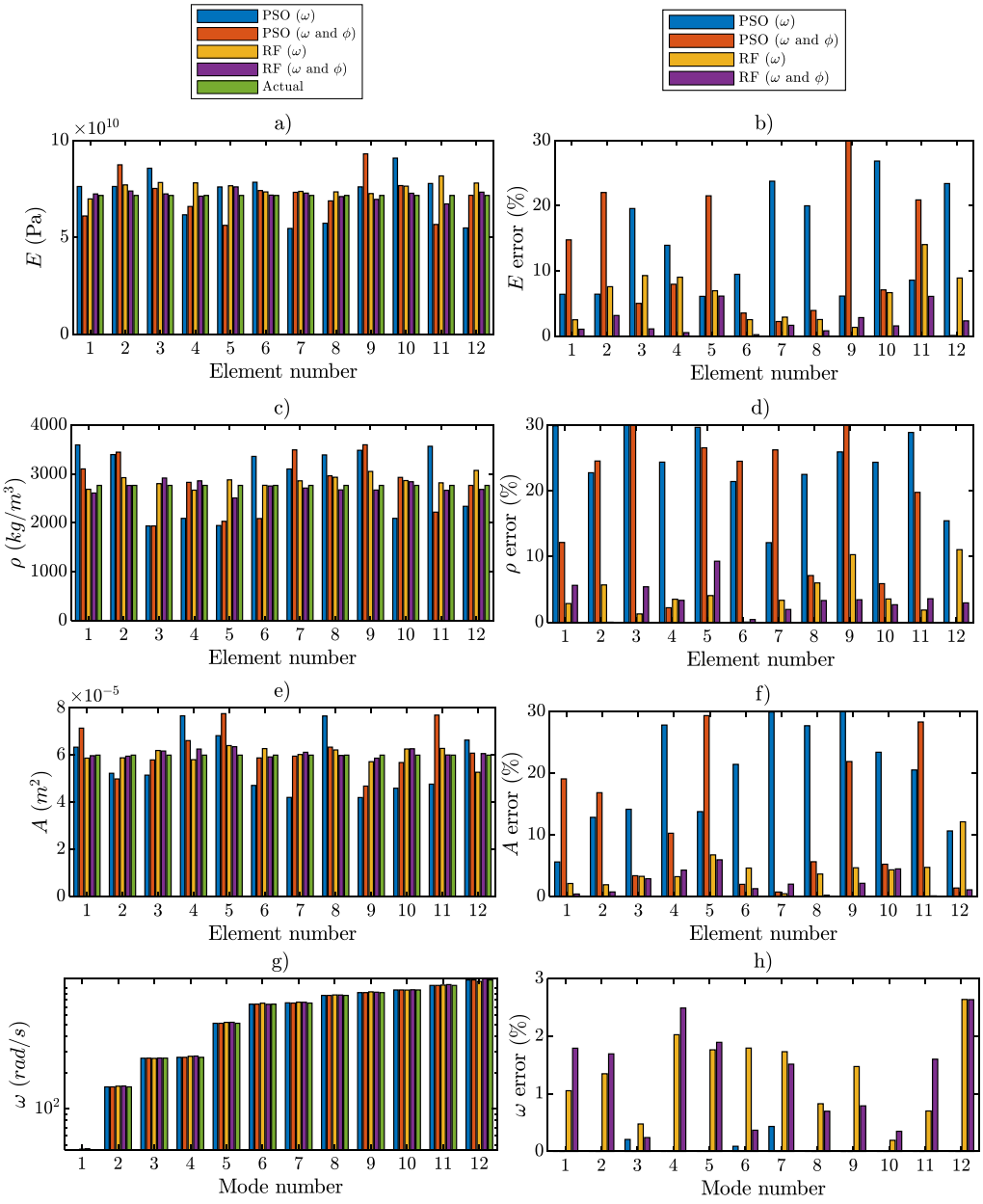

Fig. 7. Comparison between updated and actual values (left plots) and associated errors (right plots) for: (a–b) E, (c–d) ρ, (e–f) A and (g–h) ω, when using different methods. In the key, PSO (ω) and PSO (ω and ϕ) refer to the use of objective functions O_1 and O_2, respectively, and RF (ω) and RF (ω and ϕ) refer to inverse surrogate models $\hat{\mathbf{g}}_1$ and $\hat{\mathbf{g}}_2$, respectively. Note that the vertical axis of plot (g) is in log-scale. The PSO (ω and ϕ) errors in plot (h) are not visible at this vertical scale, but they are given in Fig. 5.

The results largely confirm all observations drawn in the previous section, with the proposed approach outperforming the PSO-based optimization for both scenarios including or excluding the mode shapes. The table also shows that the proposed inverse surrogate approach has a good repeatability, since its results have standard deviations consistently below 1%, and that the computational costs of the two approaches are nearly identical. It is worth noting that such computational cost is only incurred once for a given structure when using the inverse surrogate model, since once the regression model is trained any further model updating driven by a newly collected experimental sample is essentially immediate, while the PSO algorithm would need to be re-run completely.

Since on actual structures the precise estimation of high order modes poses some challenges [46,47], the results (averaged over twenty repetitions) obtained by both approaches when only the first five modal parameters are exploited are reported in Table 9. The results further confirm the superiority of the proposed inverse surrogate model, whose performance in this scenario is only

Table 5
Error (%) in the updated ρ of all elements.

Element	PSO (ω)	PSO (ω and ϕ)	RF (ω)	RF (ω and ϕ)
1	29.90	12.16	2.87	5.64
2	22.76	24.55	5.71	0.04
3	29.99	29.98	1.30	5.42
4	24.38	2.24	3.53	3.36
5	29.67	26.56	4.09	9.31
6	21.43	24.51	0.06	0.44
7	12.13	26.24	3.37	1.97
8	22.51	7.13	6.01	3.33
9	25.93	30.00	10.31	3.45
10	24.36	5.90	3.57	2.69
11	28.89	19.78	1.88	3.61
12	15.46	0.01	11.07	2.97
Mean	23.95	17.42	4.48	3.52

Table 6
Error (%) in the updated A of all elements.

Element	PSO (ω)	PSO (ω and ϕ)	RF (ω)	RF (ω and ϕ)
1	5.61	19.07	2.12	0.41
2	12.84	16.83	1.91	0.75
3	14.15	3.38	3.27	2.89
4	27.80	10.26	3.22	4.29
5	13.76	29.33	6.75	5.96
6	21.43	1.98	4.62	1.28
7	29.91	0.73	0.45	2.01
8	27.69	5.64	3.65	0.21
9	30.00	21.89	4.66	2.15
10	23.39	5.24	4.33	4.48
11	20.52	28.29	4.73	0.11
12	10.64	1.38	12.12	1.09
Mean	19.81	12.00	4.32	2.13

Table 7
Error (%) in the updated ω_i for all modes.

Mode	PSO (ω)	PSO (ω and ϕ)	RF (ω)	RF (ω and ϕ)
1	9.04e−07	0.00015	1.05	1.79
2	3.78e−06	0.00037	1.35	1.69
3	0.21	0.00050	0.48	0.24
4	1.07e−06	0.00185	2.03	2.49
5	2.74e−06	0.00092	1.76	1.89
6	0.089	0.00093	1.79	0.37
7	0.43	0.00074	1.73	1.51
8	4.52e−06	0.00031	0.83	0.69
9	5.90e−05	0.00016	1.47	0.79
10	4.53e−06	0.00058	0.19	0.34
11	1.09e−05	0.00043	0.70	1.60
12	2.50e−06	0.00026	2.64	2.63
Mean	0.06	0.00060	1.34	1.34

marginally inferior to that of Table 8. Conversely, and counter-intuitively, the results of PSO have slightly improved from those of Table 8. This likely results from the reduced possibility of "overfitting" to the diminished number of modal parameters existing in the objective functions.

Finally, the robustness of the proposed method in the presence of measurement noise is investigated. For this purpose, the first five sets of modal parameters (both ω and ϕ) are contaminated with white noise having zero mean and standard deviation equal to 5% of their original values. The results, reported in Table 10, show that the proposed inverse surrogate model performs similarly as in the noiseless scenario of Table 9, suggesting that the proposed method is robust also in the presence of measurement noise.

3.2. Case study II: IASC–ASCE structural health monitoring benchmark structure

The quarter-scale structure of the Earthquake Engineering Research Laboratory at the University of British Columbia [38], shown in Fig. 9(a), is considered as a second, experimental case-study. The structure is a four-story building with a 2.5 m by 2.5 m floor plan and a total height of 3.6 m. It is made of hot-rolled grade 300 W steel with a yield stress of 300 MPa. Each exterior face of each floor has two diagonal braces. The four floor slabs have masses of 3200, 2400, 2400 and 1600 kg, respectively from the lowest

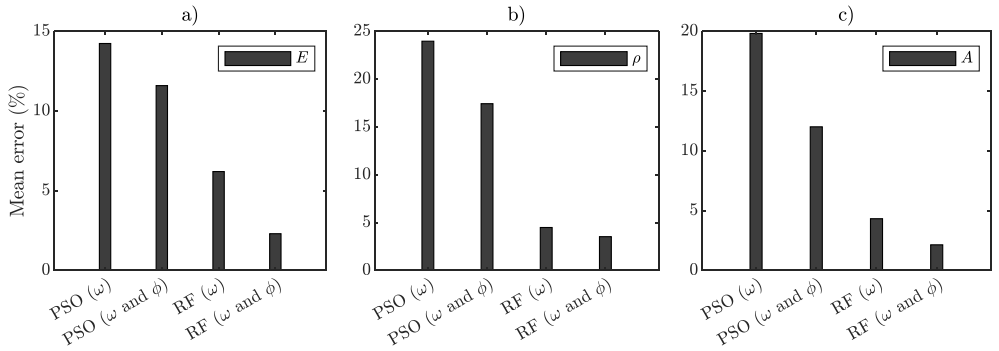

Fig. 8. Mean values of model updating errors through all elements for: (a) E, (b) ρ, and (c) A.

Table 8
Mean and standard deviation (STD) of model updating errors when all FEMU methods are repeated 20 times, and all 12 modes are considered.

Parameter	PSO (ω)		PSO (ω and ϕ)		RF (ω)		RF (ω and ϕ)	
	Mean	STD	Mean	STD	Mean	STD	Mean	STD
Error E (%)	16.64	3.47	14.28	2.83	4.09	0.82	3.46	0.83
Error ρ (%)	19.11	5.13	18.44	1.98	3.92	0.68	3.19	0.80
Error A (%)	20.23	3.66	14.49	3.30	3.82	0.77	3.54	0.93
Mean run time (sec)	3.73		21.76		4.07		18.44	

Table 9
Mean and standard deviation (STD) of model updating errors when all FEMU methods are repeated 20 times, and only the first 5 modes are considered.

Parameter	PSO (ω)		PSO (ω and ϕ)		RF (ω)		RF (ω and ϕ)	
	Mean	STD	Mean	STD	Mean	STD	Mean	STD
Error E (%)	16.78	2.98	12.52	3.33	4.05	1.13	3.67	1.31
Error ρ (%)	18.37	2.27	15.68	1.84	4.48	1.17	4.17	1.23
Error A (%)	16.81	3.03	12.87	2.84	4.22	1.27	3.90	0.68
Mean run time (sec)	1.22		21.82		4.14		13.99	

Table 10
Mean and standard deviation (STD) of model updating errors when all FEMU methods are repeated 20 times on the first 5 modes contaminated with noise.

Parameter	PSO (ω)		PSO (ω and ϕ)		RF (ω)		RF (ω and ϕ)	
	Mean	STD	Mean	STD	Mean	STD	Mean	STD
Error E (%)	18.54	4.09	14.45	2.60	5.15	1.23	4.81	0.88
Error ρ (%)	19.94	2.85	18.62	2.91	4.28	1.00	3.78	1.02
Error A (%)	18.50	2.60	14.72	2.79	4.87	1.07	4.48	0.72
Mean run time (sec)	1.37		20.82		3.21		12.27	

to the highest one. The first five natural frequencies of the structure calculated with the stochastic subspace identification (SSI) method [48] applied to ambient vibration recordings are given in [49] and are also reported in the first row of Table 13.

An open-access FEM of the structure created in *MATLAB* was provided in [50], and it is shown in Fig. 9(b–c). Columns and floor beams are modeled as Euler–Bernoulli beams, while diagonal braces are modeled as bars without bending stiffness. Each raised floor has 3 DOFs, namely the two horizontal translations and the x-y rotation, and each raised node has three additional DOFs, namely vertical motion and x-z/y-z rotations, while all ground nodes are fully fixed. This equates to a total of 120 DOFs possessed by the model. Geometrical and material properties of all structural members are given in Table 11 [50]. Note that the Table refers to strong inertia directions for columns and beams, and these are for bending about the y axis and vertically, respectively.

When the values given in Table 11 are assigned to the model, the modal frequencies listed in the second row of Table 13 are obtained, which are, on average, about 10% off from the experimental ones of the first row. Therefore, both PSO- and RF-based FEMU approaches are used to update all model parameters in order to reduce such differences. These are the 11 parameters shown in Fig. 10, which plots the results of a sensitivity analysis conducted using Eqs. (6) and (8). Note that the indices c, b, and br stand for column, beam, and brace, respectively. Although the first five modal frequencies are shown to exhibit virtually zero sensitivity to some of the parameters, such as $I_{s,b}$, J_c and J_b, these are still given as input to the FEMU procedures as it is interesting to assess whether their initial values would be left unchanged (as it would seem reasonable) or would be varied during the updating routine.

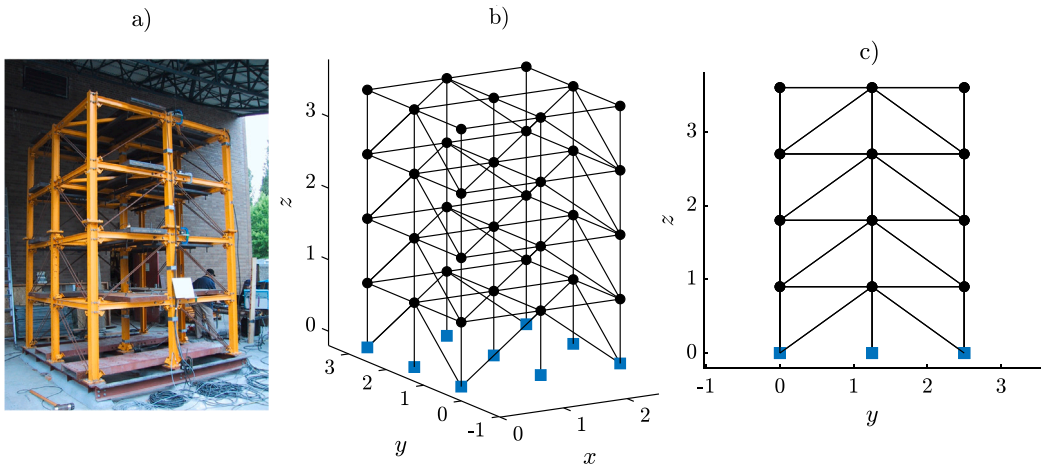

Fig. 9. Photo (a) and layout of the FEM of the IASC-ASCE benchmark structure given in [50]: (b) 3D view; (c) 2D view in the *y*-*z* plane.

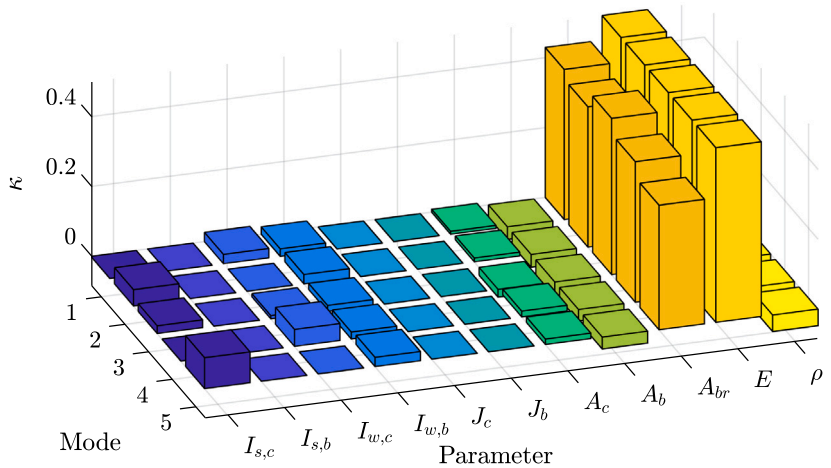

Fig. 10. Normalized sensitivity (κ) of each modal frequency to variations in the mechanical and geometrical parameters of the FEM.

Table 11
Properties of structural members.
Source: Table reproduced from [50].

Property	Columns	Floor beams	Braces
Section type	B100 × 9	S75 × 11	L25 × 25 × 3
Cross-sectional area A (m^2)	1.133×10^{-3}	1.43×10^{-3}	0.141×10^{-3}
Moment of inertia (strong direction) I_s (m^4)	1.97×10^{-6}	1.22×10^{-6}	0
Moment of inertia (weak direction) I_w (m^4)	0.664×10^{-6}	0.249×10^{-6}	0
St. Venant torsion constant J (m^4)	8.01×10^{-9}	38.2×10^{-9}	0
Young's modulus E (Pa)	2×10^{11}	2×10^{11}	2×10^{11}
Shear modulus G (Pa)	$E/2.6$	$E/2.6$	$E/2.6$
Mass per unit volume ρ (kg/m^3)	7800	7800	7800

3.2.1. Case study II: model updating using PSO and the proposed inverse surrogate model

The PSO-based FEMU procedure is performed using the five experimental frequencies listed in the first row of Table 13 to form the objective function O_1 as set in Eq. (9), and by then adjusting the design variables of Table 11 (up to a +/- 30% range of variation from their initial values) to minimize it. The algorithm was run under the settings of Table 2, which required 72.03 s of computational time, and the resulting history for the objective function O_1 is shown in Fig. 11(a).

An inverse surrogate model termed $\hat{\mathbf{g}}_3$ is created by randomly shifting the parameters of Table 11 within a +/- 30% range of variation from their initial values as the target, and by using the resulting first five modal frequencies as the independent variables. The settings of Table 3 are used to generate $\hat{\mathbf{g}}_3$, except that in this case the number of samples for the training phase was set to

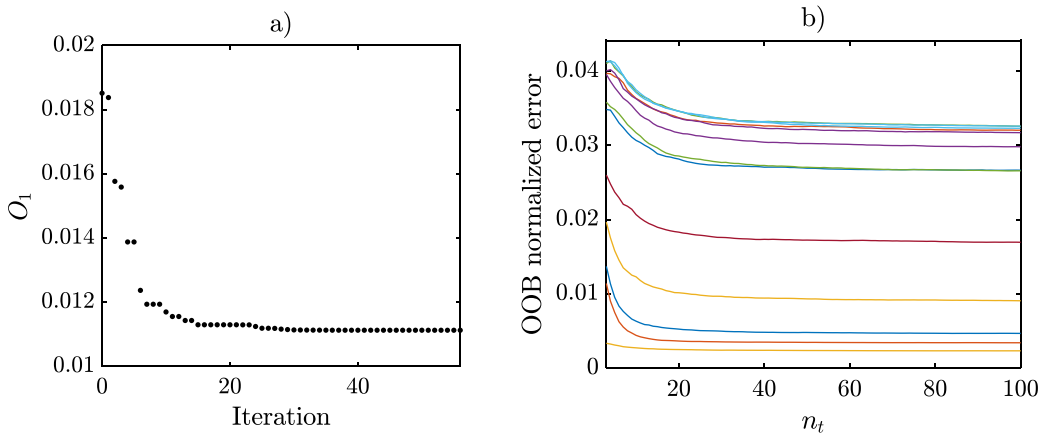

Fig. 11. (a) History of the objective function O_1 during the iteration of the PSO algorithm on case study II. (b) OOB normalized error vs. number of trees for all 11 target parameters for $\hat{\mathbf{g}}_3$.

Table 12
Design variables and their relative shift after model updating.

Design variable	Initial values	Updated values (PSO)	Shift from initial(%) (PSO) (%)	Updated values (RF)	Shift from initial (RF) (%)
$I_{s,c}$	1.970×10^{-06}	1.379×10^{-06}	30.00	1.690×10^{-06}	14.19
$I_{s,b}$	1.220×10^{-06}	1.586×10^{-06}	30.00	1.205×10^{-06}	1.24
$I_{w,c}$	6.640×10^{-07}	4.648×10^{-07}	30.00	5.887×10^{-07}	11.35
$I_{w,b}$	2.490×10^{-07}	1.743×10^{-07}	30.00	2.286×10^{-07}	8.18
J_c	8.010×10^{-09}	1.041×10^{-08}	30.00	7.973×10^{-09}	0.47
J_b	3.820×10^{-08}	4.966×10^{-08}	30.00	3.519×10^{-08}	7.89
A_c	1.133×10^{-03}	7.931×10^{-04}	30.00	9.539×10^{-04}	15.81
A_b	1.430×10^{-03}	1.001×10^{-03}	30.00	1.298×10^{-03}	9.20
A_{br}	1.410×10^{-04}	1.313×10^{-04}	6.90	1.300×10^{-04}	7.79
E	2.000×10^{11}	1.800×10^{11}	10.00	1.889×10^{11}	5.57
ρ	7800	5460	30.00	7675	1.60

5000. The training phase required a computational time of 90.39 s, and the OOB error analysis computed for the 11 target variables that is shown in Fig. 11 confirms that all errors plateau before $n_t = 100$, hence there would be no benefit by using a larger n_t value.

3.2.2. Case study II: comparison of results

Table 12 reports the updated FEM parameters and their deviations from the initial values. Although very large variations from such values would not be expected, since they were measured by the authors of [49], the table shows that the PSO method has shifted several parameters at their upper or lower admissible bound, i.e. at +/- 30%, especially those associated to low sensitivities as seen in Fig. 10. This is likely a result of the ill-conditioning issue that plagues "classic" optimization-based FEMU approaches, where similar modal results can arise from various combinations of structural properties, and therefore there is a risk of convergence towards local minima. The proposed inverse surrogate model, instead, yielded feasible deviations within the admissible range for all the parameters.

The modal frequencies associated to the updated FEMs are listed in Table 13. Similarly as for the case of "case study I", PSO yielded modal frequencies closer to the experimental ones than those resulting from the RF-based approach. All errors from PSO are lower than 5% except for the case of the third mode, which is the only torsional mode among the five considered. Nevertheless, the modal frequencies associated to the FEM updated by the proposed inverse surrogate model are still significantly improved from the initial ones, since all errors are at least halved, except, as in the case of PSO, for the third frequency.

3.2.3. Case study II: robustness of the results

To investigate the robustness of the results, both procedures described in Section 3.2.1 were repeated 20 times in order to take into account the influence of the random initialization of both approaches. The results are presented in Tables 14 and 15. The latter confirm all conclusions drawn in the previous section, and the standard deviations associated to the proposed inverse surrogate models are relatively low, with all values at or below 4% in Table 14, and below 1% in Table 15, hence demonstrating a good repeatability.

Table 13
Modal frequencies of the IASC-ASCE benchmark structure. The experimental ones are courtesy of [49]. The "initial FEM" are obtained using the FEM with the parameters given in [50].

Parameter	f_1	f_2	f_3	f_4	f_5
Experimental (Hz)	7.49	7.76	14.49	19.89	21.01
Initial FEM (Hz)	8.20	8.53	13.95	22.54	24.24
PSO (Hz)	7.57	7.81	13.19	20.58	21.87
RF (Hz)	7.68	7.96	13.13	21.05	22.55
Initial FEM error (%)	9.53	9.89	3.72	13.31	15.36
PSO error (%)	1.02	0.60	8.99	3.47	4.11
RF error (%)	2.53	2.61	9.39	5.84	7.31

Table 14
Mean and standard deviation (STD) of model updating errors when all FEMU methods are repeated 20 times.

Design variable	Mean PSO shift from initial (%)	STD PSO shift from initial (%)	Mean RF shift from initial (%)	STD RF shift from initial (%)
$I_{s,c}$	30.00	4.33×10^{-05}	15.58	2.51
$I_{s,b}$	29.28	2.24×10^{0}	3.05	2.29
$I_{w,c}$	30.00	6.25×10^{-04}	11.45	3.09
$I_{w,b}$	30.00	3.50×10^{-05}	5.43	3.29
J_c	28.49	6.22×10^{0}	3.05	1.65
J_b	29.99	2.67×10^{-02}	3.91	2.48
A_c	30.00	2.24×10^{-07}	17.68	2.61
A_b	30.00	2.35×10^{-04}	7.86	3.63
A_{br}	6.90	1.13×10^{-02}	9.38	1.46
E	10.00	1.04×10^{-06}	5.02	0.85
ρ	30.00	4.40×10^{-04}	10.81	4.06

Table 15
Mean and standard deviation (STD) of modal frequency errors when all FEMU methods are repeated 20 times.

Mode	Mean PSO error (%)	STD PSO error (%)	Mean RF error (%)	STD RF error (%)
1	1.02	5.34×10^{-03}	2.48	0.73
2	0.61	5.02×10^{-03}	2.55	0.75
3	8.99	4.94×10^{-03}	9.20	0.73
4	3.47	5.12×10^{-03}	5.78	0.72
5	4.11	4.63×10^{-03}	7.22	0.78

4. Conclusions

This article proposes a method for deterministic finite element model updating based on a so-called "inverse surrogate model", which is represented by a random forest algorithm for regression where the independent variables are a set of structural responses, and the target variables are geometric and mechanical properties of the structural elements. The approach is computationally efficient, as computational costs are related to the RF training phase only, while inference following any new set of experimental modal parameters is immediate.

The performance of the proposed method was compared to that offered by the widely used PSO algorithm on a numerical and an experimental dataset where the structural responses are represented by a set of modal parameters. The results show that this approach is less susceptible to ill-conditioning issues, characteristic of deterministic FEMU procedures, for which similar structural responses can arise from various combinations of structural properties (see e.g. [32]). This occurs since optimization methods tends to focus only on minimizing an objective function based on the disparity between experimental and model-derived modal parameters, typically neglecting the mutual relations between the latter, therefore increasing the risk to convergence to local minima. In fact, on both case studies, although the PSO-based updated modal parameters are closer to the experimentally measured ones, the predictions of the geometric and mechanical properties of the structure made by the proposed inverse surrogate model are significantly more accurate than those given by PSO. The robustness of the proposed method was also tested by re-running each computation 20 times with random initialization, and the results indicate a good repeatability since the standard deviation in the estimation of each structural parameters was contained within a 1% and a 4% range in the first (numerical) and the second (experimental) case study, respectively.

CRediT authorship contribution statement

S. Kamali: Conceptualization, Data curation, Formal analysis, Investigation, Methodology, Software, Validation, Visualization, Writing – original draft. **S. Mariani:** Methodology, Investigation, Validation, Visualization, Writing – review & editing. **M.A.**

Hadianfard: Methodology, Validation, Writing – review & editing, Supervision. **A. Marzani:** Methodology, Validation, Writing – review & editing, Funding acquisition, Supervision.

Declaration of competing interest

The authors declare that they have no known competing financial interests or personal relationships that could have appeared to influence the work reported in this paper.

Data availability

Data will be made available on request.

Acknowledgments

- This study was carried out within the "Quantifying the effects of Structure–Soil–Structure interaction on structural modal parameters by combining Earth observation data with on-site dynamic monitoring: an enhanced vibration-based Structural Health Monitoring approach – SAT4SHM" project – funded by European Union – Next Generation EU within the PRIN 2022 PNRR program (D.D.1409 del 14/09/2022 Ministero dell'Università e della Ricerca). This manuscript reflects only the authors' views and opinions and the Ministry cannot be considered responsible for them.
- S.M. is grateful to the "Programma per Giovani Ricercatori Rita Levi Montalcini year 2020" (grant PGR20WNZMY) of the Italian Ministry of University and Research (MUR) for the financial support.

References

[1] E. Figueiredo, J. Brownjohn, Three decades of statistical pattern recognition paradigm for SHM of bridges, Struct. Health Monit. 21 (6) (2022) 3018–3054.
[2] S. Kamali, S. Quqa, A. Palermo, A. Marzani, Reducing false alarms in structural health monitoring systems by exploiting time information via Binomial Distribution Classifier, Mech. Syst. Signal Process. 207 (2024) 110938.
[3] S. Mariani, A. Kalantari, R. Kromanis, A. Marzani, Data-driven modeling of long temperature time-series to capture the thermal behavior of bridges for SHM purposes, Mech. Syst. Signal Process. 206 (2024) 110934.
[4] M. Friswell, J.E. Mottershead, Finite Element Model Updating in Structural Dynamics, vol. 38, Springer Science & Business Media, 1995.
[5] R. Brincker, C. Ventura, Introduction to Operational Modal Analysis, John Wiley & Sons, 2015.
[6] S. Ereiz, I. Duvnjak, J.F. Jiménez-Alonso, Review of finite element model updating methods for structural applications, in: Structures, Vol. 41, Elsevier, 2022, pp. 684–723.
[7] S. Bi, M. Beer, S. Cogan, J. Mottershead, Stochastic model updating with uncertainty quantification: an overview and tutorial, Mech. Syst. Signal Process. 204 (2023) 110784.
[8] Y. Govers, M. Link, Stochastic model updating—Covariance matrix adjustment from uncertain experimental modal data, Mech. Syst. Signal Process. 24 (3) (2010) 696–706.
[9] J.L. Beck, L.S. Katafygiotis, Updating models and their uncertainties. I: Bayesian statistical framework, J. Eng. Mech. 124 (4) (1998) 455–461.
[10] S. Moradi, L. Fatahi, P. Razi, Finite element model updating using bees algorithm, Struct. Multidiscip. Optim. 42 (2010) 283–291.
[11] D.T. Pham, A. Ghanbarzadeh, E. Koç, S. Otri, S. Rahim, M. Zaidi, The bees algorithm—a novel tool for complex optimisation problems, in: Intelligent Production Machines and Systems, Elsevier, 2006, pp. 454–459.
[12] J.H. Holland, Adaptation in Natural and Artificial Systems: An Introductory Analysis with Applications to Biology, Control, and Artificial Intelligence, MIT Press, 1992.
[13] J. Kennedy, R. Eberhart, Particle swarm optimization, in: Proceedings of ICNN'95-International Conference on Neural Networks, Vol. 4, IEEE, 1995, pp. 1942–1948.
[14] J.D. Collins, G.C. Hart, T. Hasselman, B. Kennedy, Statistical identification of structures, AIAA J. 12 (2) (1974) 185–190.
[15] T. Marwala, Finite-Element-Model Updating Using Computional Intelligence Techniques: Applications to Structural Dynamics, vol. 1, Springer, 2010.
[16] J.A. Nelder, R. Mead, A simplex method for function minimization, Comput. J. 7 (4) (1965) 308–313.
[17] X. Zhang, R.X. Gao, R. Yan, X. Chen, C. Sun, Z. Yang, Multivariable wavelet finite element-based vibration model for quantitative crack identification by using particle swarm optimization, J. Sound Vib. 375 (2016) 200–216.
[18] S. Qin, Y. Zhang, Y.-L. Zhou, J. Kang, Dynamic model updating for bridge structures using the kriging model and PSO algorithm ensemble with higher vibration modes, Sensors 18 (6) (2018) 1879.
[19] R. Ferrari, D. Froio, E. Rizzi, C. Gentile, E.N. Chatzi, Model updating of a historic concrete bridge by sensitivity-and global optimization-based Latin Hypercube Sampling, Eng. Struct. 179 (2019) 139–160.
[20] M. Girardi, C. Padovani, D. Pellegrini, L. Robol, A finite element model updating method based on global optimization, Mech. Syst. Signal Process. 152 (2021) 107372.
[21] D. Li, J. Zhang, Finite element model updating through derivative-free optimization algorithm, Mech. Syst. Signal Process. 185 (2023) 109726.
[22] Q. Kong, J. Gu, B. Xiong, C. Yuan, Vision-aided three-dimensional damage quantification and finite element model geometric updating for reinforced concrete structures, Comput.-Aided Civ. Infrastruct. Eng. (2023).
[23] M. Jahangiri, M.A. Hadianfard, M.A. Najafgholipour, M. Jahangiri, M.R. Gerami, Interactive autodidactic school: A new metaheuristic optimization algorithm for solving mathematical and structural design optimization problems, Comput. Struct. 235 (2020) 106268.
[24] M. Girardi, C. Padovani, D. Pellegrini, M. Porcelli, L. Robol, Finite element model updating for structural applications, J. Comput. Appl. Math. 370 (2020) 112675.
[25] I. Behmanesh, B. Moaveni, G. Lombaert, C. Papadimitriou, Hierarchical Bayesian model updating for structural identification, Mech. Syst. Signal Process. 64 (2015) 360–376.
[26] Y. Bai, Z. Peng, Z. Wang, A finite element model updating method based on the trust region and adaptive surrogate model, J. Sound Vib. 555 (2023) 117701.
[27] R. Perera, S. Sandercock, A. Carnicero, Civil structure condition assessment by a two-stage FE model update based on neural network enhanced power mode shapes and an adaptive roaming damage method, Eng. Struct. 207 (2020) 110234.

[28] Y. Yuan, F.T. Au, D. Yang, J. Zhang, Active learning structural model updating of a multisensory system based on Kriging method and Bayesian inference, Comput.-Aided Civ. Infrastruct. Eng. 38 (3) (2023) 353–371.
[29] J. Zeng, Y.H. Kim, S. Qin, Bayesian model updating for structural dynamic applications combing differential evolution adaptive Metropolis and Kriging model, J. Struct. Eng. 149 (6) (2023) 04023070.
[30] C. He, Z. Li, H. He, J. Wang, Stochastic dynamic model updating of aerospace thermal structure with a hierarchical framework, Mech. Syst. Signal Process. 160 (2021) 107892.
[31] P. Ni, Q. Han, X. Du, X. Cheng, Bayesian model updating of civil structures with likelihood-free inference approach and response reconstruction technique, Mech. Syst. Signal Process. 164 (2022) 108204.
[32] E. Simoen, G. De Roeck, G. Lombaert, Dealing with uncertainty in model updating for damage assessment: A review, Mech. Syst. Signal Process. 56 (2015) 123–149.
[33] B. Titurus, M. Friswell, Regularization in model updating, Int. J. Numer. Methods Eng. 75 (4) (2008) 440–478.
[34] X. Li, S. Law, Adaptive Tikhonov regularization for damage detection based on nonlinear model updating, Mech. Syst. Signal Process. 24 (6) (2010) 1646–1664.
[35] R. Moradi, R. Berangi, B. Minaei, A survey of regularization strategies for deep models, Artif. Intell. Rev. 53 (2020) 3947–3986.
[36] L. Breiman, Random forests, Mach. Learn. 45 (2001) 5–32.
[37] S. Kamali, M.A. Hadianfard, Spectral optimization-based modal identification: A novel operational modal analysis technique, Mech. Syst. Signal Process. 198 (2023) 110445.
[38] E.A. Johnson, H.-F. Lam, L.S. Katafygiotis, J.L. Beck, Phase I IASC-ASCE structural health monitoring benchmark problem using simulated data, J. Eng. Mech. 130 (1) (2004) 3–15.
[39] N. Meinshausen, G. Ridgeway, Quantile regression forests, J. Mach. Learn. Res. 7 (6) (2006).
[40] T. Hastie, R. Tibshirani, J. Friedman, The Elements of Statistical Learning: Data Mining, Inference, and Prediction, in: Springer Series in Statistics, Springer, 2009.
[41] O.Z. Maimon, L. Rokach, Data Mining with Decision Trees: Theory and Applications, vol. 81, World scientific, 2014.
[42] R. Genuer, J.-M. Poggi, R. Genuer, J.-M. Poggi, Random forests, Springer, 2020.
[43] A. Cutler, D.R. Cutler, J.R. Stevens, Random forests, in: Ensemble machine learning: Methods and applications, Springer, 2012, pp. 157–175.
[44] T.M. Oshiro, P.S. Perez, J.A. Baranauskas, How many trees in a random forest? in: Machine Learning and Data Mining in Pattern Recognition: 8th International Conference, MLDM 2012, Berlin, Germany, July 13-20, 2012. Proceedings 8, Springer, 2012, pp. 154–168.
[45] M. Jahangiri, M.A. Hadianfard, Vibration-based structural health monitoring using symbiotic organism search based on an improved objective function, J. Civ. Struct. Health Monit. 9 (5) (2019) 741–755.
[46] E. Reynders, J. Houbrechts, G. De Roeck, Fully automated (operational) modal analysis, Mech. Syst. Signal Process. 29 (2012) 228–250.
[47] M. Jahangiri, A. Palermo, S. Kamali, M.A. Hadianfard, A. Marzani, A procedure to estimate the minimum observable damage in truss structures using vibration-based structural health monitoring systems, Probab. Eng. Mech. 73 (2023) 103451.
[48] P. Van Overschee, B. De Moor, Subspace Identification for Linear Systems: Theory—Implementation—Applications, Springer Science & Business Media, 2012.
[49] S. Dyke, Report on the building structural health monitoring problem phase 2 experimental, 2011, URL https://datacenterhub.org/resources/2812.
[50] S. Dyke, Report on the building structural health monitoring problem phase 1 analytical, 2011, URL https://datacenterhub.org/resources/2806.